Asian Journal of Chemistry; Vol. 33, No. 6 (2021), 1208-1214

ASIAN JOURNAL OF CHEMISTRY

https://doi.org/10.14233/ajchem.2021.23134

Synthesis and Physico-chemical Characterization of Solid Solution (1-*x*)CCTO–*x*$PbTiO_3$

M. Slaoui[1,2], N. Gouitaa[2], A. Lahrichi[2], A. Harrach[1], M. Haddad[3] and T. Lamcharfi[2,*]

[1]Condensed Matter Chemistry Laboratory, Sidi Mohammed Ben Abdellah University, BP 2202, Route d'Imouzzer, Faculty of Science and Technology of Fez, BP 2202, Fez, Morocco
[2]Signals, Systems and Components Laboratory, Sidi Mohammed Ben Abdellah University, BP 2202, Route d'Imouzzer, Faculty of Science and Technology of Fez, BP 2202, Fez, Morocco
[3]Materials and Archaeomaterials Spectrometry Laboratory (LASMAR), research unit associated with CNRST (URAC11), Moulay-Ismail University, Faculty of Sciences, 50000 Meknès, Maroc

*Corresponding author: E-mail: lamcharfi_taj@yahoo.fr

Received: 23 January 2021; *Accepted*: 16 March 2021; *Published online*: 5 June 2021; AJC-20345

The composite materials of (1-*x*)$CaCu_3Ti_4O_{12}$, *x*$PbTiO_3$((1-*x*)CCTO–*x*PT) were prepared by a modified solid-state method in several steps. The Rietveld refinement indicates the formation of the pure cubic and tetragonal phases for calcium copper titanate (CCTO) and lead-titanate (PT) pure ceramics, respectively. While for CCTO-PT composites, the coexistence of the two cubic and tetragonal phases was detected with the space group *Im*-3 and *P*4mm, respectively. The Raman spectra confirmed these phase formations. The SEM images indicated a change in grains shape from quadratic to semi-spherical with increases of PT contents and a reduce in average grains size with increase of PT content. The dielectric measurements as function of temperature showed two anomalies which exhibit a relaxation-like phenomenon and a clear diffuseness behaviour for all the samples. In addition, the conductivity of these materials decreases and the resistance of grain boundaries was found to increase with the increase of PT addition.

Keywords: Solid-state, Relaxation, Diffuseness, Conductivity, Grain boundaries.

INTRODUCTION

There are large number of applications for ceramic materials due to their giant relative permittivity, electrical insulating and electrical conducting properties. Actually, advanced ceramics such as calcium copper titanate $CaCuTi_4O_{12}$ (CCTO) has become more and more used for the manufacture of microelectronic circuits [1,2]. It is widely used in the treatment of radioactive wastes since these perovskite showed a good immobilizing the nuclear wastes [3-6]. Recent studies [7,8] reported that the dielectric constant of $CaCuTi_4O_{12}$ ceramic is about 10^5 at room temperature independence between 1000 and 600 K. The dielectric permittivity remains almost constant as function of frequency in a range of frequencies from 50 Hz to 20^6 Hz. These dielectric properties have made CCTO a very useful material in the field of microelectronics such as capacitors and memory devices. Despite the fact that the values of its dielectric constant, which is very large, are not well understood. It is known that the high dielectric response is related with extrinsic effects [9].

Lead titanate ($PbTiO_3$, PT) is perovskite type ferroelectric material, which has a high curie point (T_c) of 490 ºC and a large tetragonality of c/a = 1.064 and a small relative permittivity of e/e_0 = 200 [10], spontaneous polarization, pyroelectric and piezoelectric properties [11]. These properties make it a material applicable in many devices such as ultransonic transducers [12], thermistors, optical electronic devices and satellite detections [13]. At room temperature, $PbTiO_3$ crystallizes in tetragonal perovskite structure [14] and combined with other oxides it forms materials such as $PbLaTiO_3$ (PLT), $Pb(ZrTi)O_3$ (PZT) and (PbLa) $(ZrTi)O_3$ (PLZT) [15].

Many researchers have studied the processing of $PbTiO_3$ powders by different methods such as sol gel [16], co-precipitation [17], hydrothermal reaction [18]. Ultrafine $PbTiO_3$ precursor powders with high chemical homogeneity and purity can be synthesized by varying the various processing parameters in each chemical route [19].

In this work, (1-*x*)CCTO–*x*PT (x = 0 to100%) ceramics were prepared by hybrid method. The study of the effect of lead titanate (PT) on the structural, dielectric and electrical properties of CCTO with is effect on the nature of transition phase (1-*x*)CCTO–*x*PT was carried out and the results obtained were discussed.

EXPERIMENTAL

The solid solution (1-x) CCTO–*x*PT was prepared by solid state modified method with several steps. In the first step, lead titanate was prepared by sol-gel methd using lead acetate (99% purity), $Ti\{OCH(CH_3)_2\}_4$ (97% purity) and lactic acid as the starting materials. In this method, stochiometric of lead acetate dissolved in distilled water to obtain a homogenous solution (solution 1) followed by the addition of sol titanium isopropoxide in stochiometric amounts to the solution 1 to get solution 2 (lead titanate (PT)).

The PT solution was stirred 1h for homogenization and heated at 80 ºC in oven for 48 h to obtain a xerogel. The xerogel was grounded for 30 min and the powder obtained was calcined at 700 ºC for 4 h. In the second step, CCTO was synthesized with solid state and the precursors were $CaCO_3$, CuO and TiO_2 with high purity. The raw powders for each concentration were mixed in an agate mortar for 1 h and stirred in acetone for 3 h. Then the obtained powder was calcined at 1050 ºC for 4 h.

In the final step, [(1-*x*)CCTO–*x*PT] was obtained by mixing the CCTO and PT in a stoichiometric proportion. The resulting powders were pressed into pellets and sintered at 1000 ºC for 4 h. The XRD and the Rietveld refinement were used to study the structure of compounds. The crystallographic analysis was carried using the diffractometer (X Pert-Pro). The data recording is performed over 5-100º. This type of recording allowed to use subsequent refine structure by the Rietveld method as well as the parameters and the group of space of the mesh on the positions of the atoms in the structure. The Raman spectrum was recorded at room temperature.

To study the electric and dielectric properties, the sides of the pellets were metallized with a thin layers of silver lacquer to form a flat capacitor. The investigations of the microstructure of the pellets were performed using by a scanning electron microscope (SEM). The capacitance was measured using an HP 4284A impedance meter operating in the interval frequency of 20 Hz to 2 MHz and the temperature from room temperature to 500 ºC.

RESULTS AND DISCUSSION

XRD study: Fig. 1a shows the X-ray diffractogram obtained on pure CCTO, calcined at 1050 ºC for 4 h. It is observed that the CCTO was well crystallized without having the secondary phases. Using Rietveld refinement (Fig. 1b), the phase result shows the formation of cubic phase of CCTO with *Im*-3 space group (Table-1), which also confirmed from the literature [20].

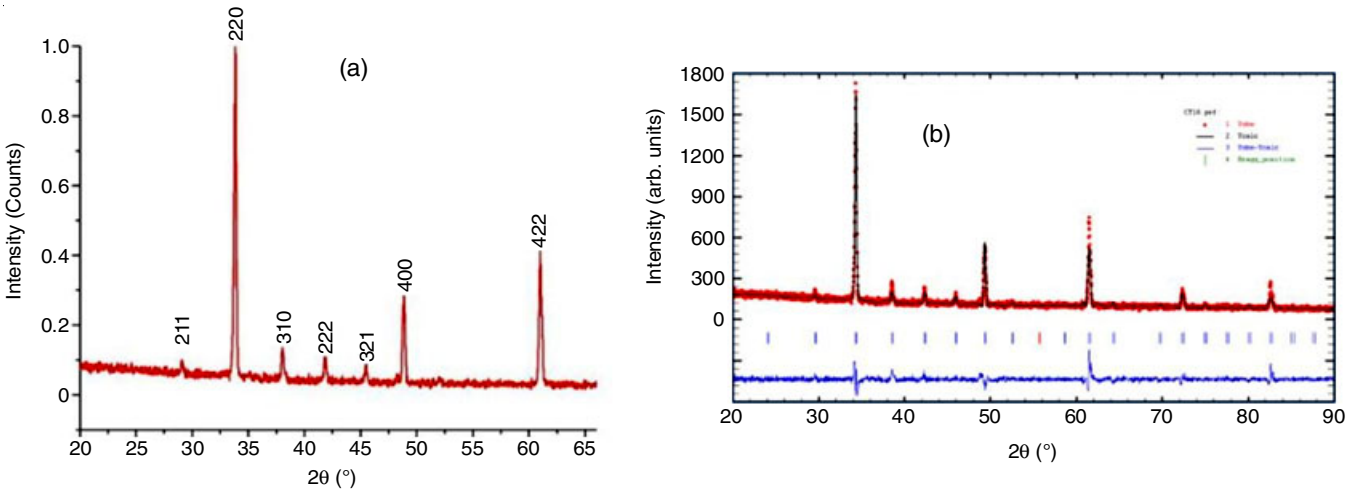

Fig. 1. X-ray diffractograms of CCTO powder obtained calcined at 1050 ºC (4 h) (a) and PT powder obtained by Ritveld (b)

TABLE-1
REFINED STRUCTURAL PARAMETERS OF THE POWDER OF (1-*x*) CCTO-*x* PT

X	Cubic phase (*Im*-3)		Tetragonal phase (*P*4mm)		
	a = b = c (Å)	Volume (Å^3)	a = b (Å)	C (Å)	Volume (Å^3)
0	7.3852	402.7942	–	–	–
10	7.3811	402.1270	–	–	–
20	7.3787	401.7350	–	–	–
30	7.3854	402.8302	3.8352	4.2043	61.8400
40	7.3910	403.7472	3.9045	4.1000	62.5049
60	7.3850	402.7648	3.9970	4.1402	66.14387
70	7.3874	403.1576	4.0046	4.1389	66.3459
80	7.3893	403.4687	4.0910	4.1371	69.2390
90	7.4010	405.3883	3.9820	4.1352	65.5800
100	–	–	3.9073	4.1336	63.1063

The XRD diffractogram of pure lead titanate (PT, Fig. 2a) confirmed a pure perovskite phase. The peaks obtained from Rietveld method (Fig. 2b) shows that all the diffraction peaks of PT were indexed with the tetragonal phase having *P*4mm space group. Present results are in good agreement with the literature [21].

The X-ray diffraction patterns of (1-*x*)CCTO–*x* PT (*x* = 0.00 to 1.00) powders (Fig. 3a) shows that for *x* = 0% (CCTO), the powder crystallizes in the pure cubic perovskite phase. For *x* = 10%, the XRD shows no change as compared with CCTO pattern. While at *x* = 20%, we can observe an appearance of a new characterization peaks. All these peaks are indexed in the tetragonal phase of lead titanate (PT) (Fig. 3b), which began to appear besides to the cubic phase of CCTO. With the increasing lead titanate (PT) contents above 20%, there are coexistence of tetragonal and cubic phase related to PT and CCTO, respectively. And the peaks intensities of tetragonal phase increase with the increasing PT content and those of cubic phase decrease and finally disappeared completely at *x* = 100%.

SEM analysis: The scanning electron microscopy (SEM) micrographs of (1-*x*)CCTO–*x*PT sintered at 1000 ºC for 4 h are shown in Fig. 4. It is well observed from the figure that for *x* = 0 to 60%, the grain form is homogenous with quadratic shape. While at above 60%, the irregular morphology with various forms of the grains is evidently visible. However, an appearance of semi-spherical grain with the coexistence of quadratic grains may be related to the coexistence of two phases tetragonal and cubic as detected in the XRD diffractogram. On the other hand, it is clear that an average grain size decreases with the increase PT contents (Table-2). This decrease is significant for high values of PT (*x* = 80 and 90%).

TABLE-2
AVERAGE GRAIN SIZE OF (1-*x*) CCTO-*x* PT CERAMICS

PT content (%)	Average grain size (μm)
10	6.93
20	4.95
30	4.39
40	4.28
50	4.09
60	3.51
70	3.27
80	1.22
90	1.13

Raman studies: The Raman spectroscopy analysis of (1-*x*)-CCTO–*x*PT (*x* = 0 to 100%) ceramics is shown in Fig. 5. For CCTO ceramic (*x* = 0%), the Raman spectrum indicates the presence of seven peaks which are also predicted by LDC (lattice dynamics calculations) as reported by Kolev *et al.* [22,23] and with the experimental values obtained. The A_g symmetry (TiO_6 rotation like) are indicated by the two bands at 448 and 509

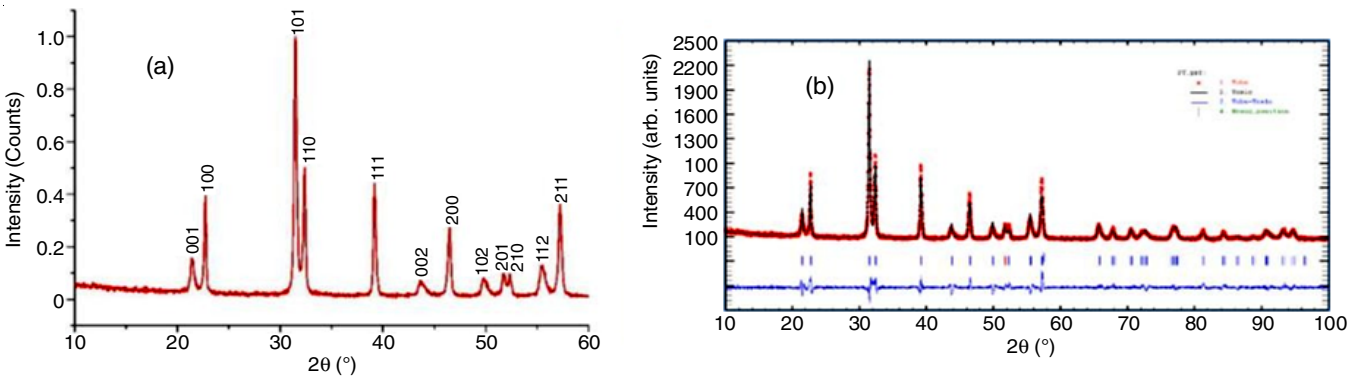

Fig. 2. (a) X-ray diffractogram of PT powder calcined at 700 °C (4 h); (b) X-ray diffractogram of PT powder obtained by Rietveld

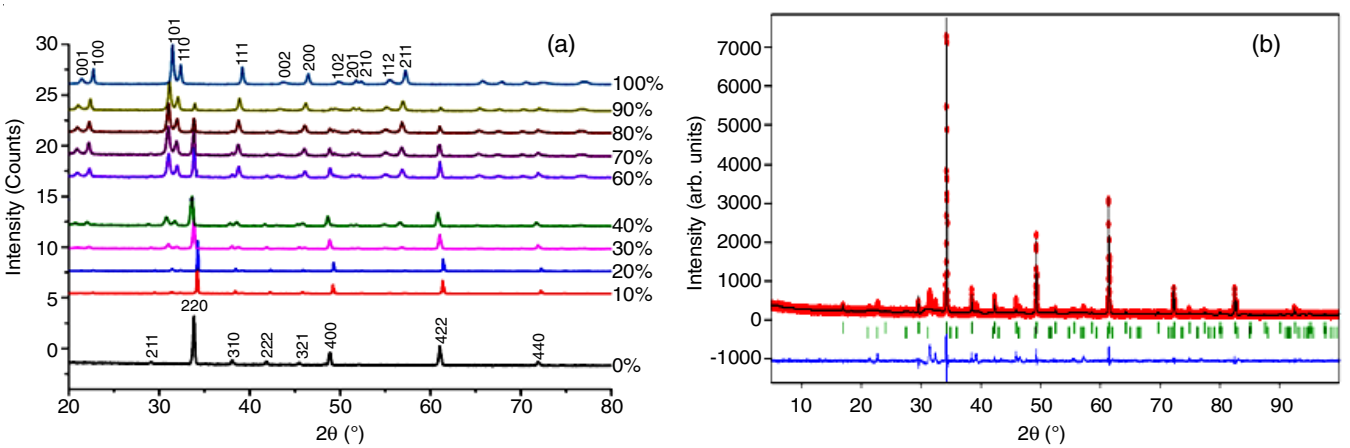

Fig. 3. (a) Characterization by XRD of the different compositions of (1-*x*) CCTO-*x*PT (*x* = 0-100); (b) X-ray diffractogram of the powder of (1-*x*) CCTO-*x* PT (x = 20%)

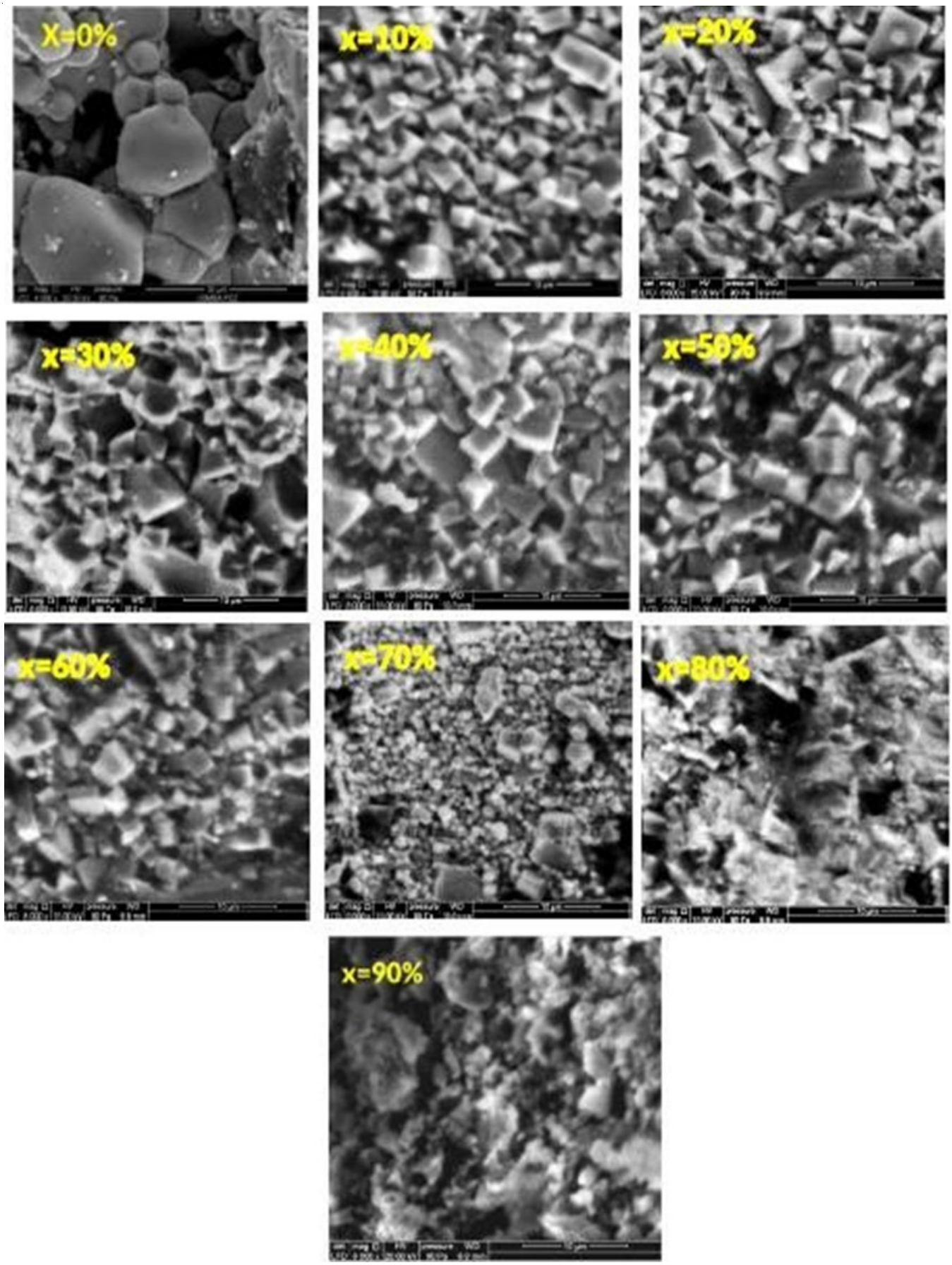

Fig. 4. SEM images of (1-*x*)CCTO-*x* PT ceramics, sintered at 1000 °C for 4 h

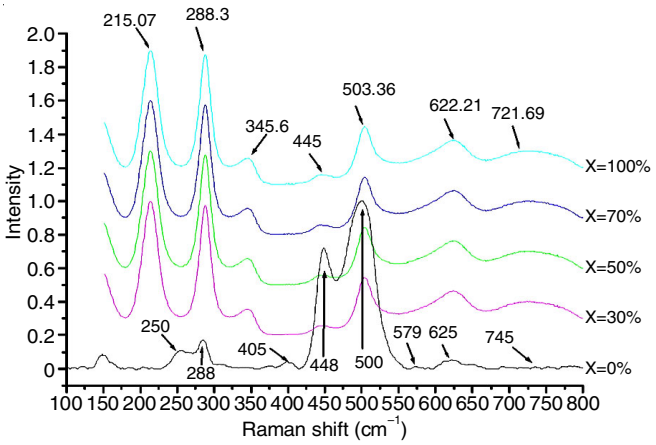

Fig. 5. Raman spectra of (1-*x*)CCTO-*x* PT powders

cm^{-1}. And the band at 579 cm^{-1} is attributed to F_g symmetry mode (O-Ti-O anti stretching) [24]. While the band at 250 cm^{-1} is related to CuO [25] but does not appear in our XRD results.

With the increase content of PT, it was observed that an appearance of seven new bands at 215.07, 288.31, 345.6, 445, 503, 622 and 721 cm^{-1} assigned to {E(2TO), B_1 + E, A_1(2TO), E(2LO) + A(2LO), E(3TO), A1(3TO) and E(3TO) + A1(3TO)}, respectively. All these bands are attributed to the tetragonal phase of PT powder [25,26]. From *x* = 30 to 70%, the intensity of tetragonal PT phase increases while for CCTO bands decreases. And at *x* = 100%, all the peaks are assigned to the tetragonal PT phase.

Dielectric properties: The evolution of the dielectric constant *versus* temperature (room temperature-600 ºC) of the (1-*x*)CCTO–*x*PT (for *x* = 0 to 100%) at different frequencies (Fig. 6). With the increase of temperature, the dielectric constant increase up to T_m then systems become paraelectric and the dielectric constant decreases. It was also observed the two dielectric anomalies T_1 and T_2 for all the prepared ceramics. These two anomalies shift to the high temperature with the increase of frequencies indicating a relaxor-like behaviour. The relaxation behaviour is attributed to the PT addition, which causes a micro-inhomogeneity [26,27]. To understand the nature of this transition many researches are still under investigation. These relaxor behaviour was also reported recently by Dong *et al.* [28] for $BiScO_3$-$PbTiO_3$ ceramics.

As shown in Table-3, the first dielectric anomaly at T_1 is observed at lower temperature about 311 ºC and shifts to the lower temperature with increasing of PT contents. And the dielectric constant value corresponding decreases with the increase of PT content from 10 to 90%. While the second anomaly at temperature T_2 superior to T_1 is related to the phase transition

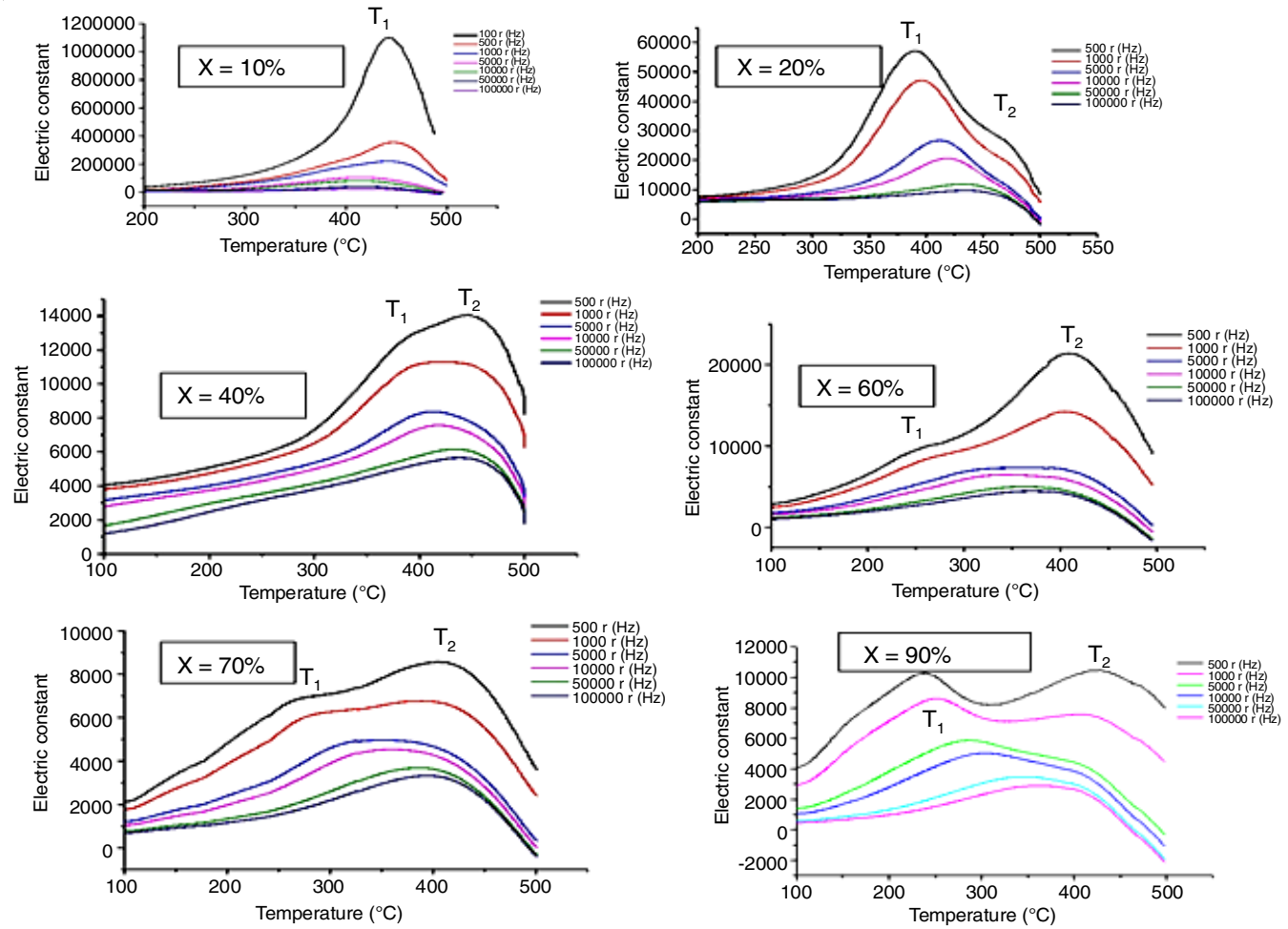

Fig. 6. Evolution of the dielectric constant, at different frequencies, as a function of temperatures for (1-*x*) CCTO-*x* PT (*x* = 10-100%) sintered at 1000 °C for 4 h

TABLE-3
DIELECTRIC CONSTANT AND TEMPERATURE TRANSITION OF THE TWO ANOMALIES OF (1-*x*) CCTO-*x*PT CERAMICS SINTERED AT 550 Hz

X (%)	ε'_{max}		Tmax (°C)	
	ε'_{max1}	ε'_{max2}	T_1	T_2
0	100228	–	360	–
20	57073	26962	391	468
40	12964	14068	395	446
60	7503	12466	337	461
70	5703	6471	268	471
90	10049	122117	237	480

of PT. It is also observed a fluctuate evolution of T_2 and the dielectric constant correspondent for all the samples (Table-3).

The dielectric transition has a large character showing a diffuse behaviour especially for $x = 40\%$ and 70% of PT content. The broad dielectric phase transition is due to the PT addition, which change the tetragonality of the samples, so different Curie temperatures present a broad dielectric transition in these ceramics [29].

The degree of relaxation behaviour could be estimated by the empirical parameter:

$$\Delta Ti = Ti(5000\ Hz) - Ti\ (500\ Hz)$$

where Ti (500 Hz) and Ti (5000 Hz) are temperatures correspond to the maximum dielectric constant at frequencies of 500 Hz and 5000 Hz, respectively. The Ti value was calculated for all samples (Table-4). It is observed that as x increases, ΔT_1 and ΔT_2 are greater than 0 until, it reaches a maximum value at $x = 90\%$. This means that the two phases transition T_1 and T_2 exhibit a relaxation phenomenon, which became very important at $x = 90\%$ of PT content.

TABLE-4
TEMPERATURE DIFFERENCE BETWEEN 5000 Hz AND 500 Hz AS A FUNCTION OF x FOR (1-x)CCTO-xPT (x = 10-90%)

X (%)	ΔT_1 500 (Hz)	ΔT_2 5000 (Hz)
10	27	–
20	22	2
40	23	12
60	27	14
70	17	9
90	45	22

To obtain more detail on conduction and relaxation behaviour of (1–x)CCTO–xPT ceramics, the log real part of AC conductivity *vs.* frequency at 320 ºC was studied. For all samples, the frequency conductivity spectra indicates two regions–one in the lower frequency and the other in the higher frequency (Fig. 7). At lower frequencies, the conductivity is almost constant as function of frequency because the electric field cannot change the movement of charge carriers. This region is related to the grain boundary effect. While in the high frequencies region, the conductivity indicated frequency dispersion, which is due to the hopping of high weight charge. On the other hand, the addition of PT caused a decrease in conductivity, this behaviour is perhaps related to the lower electrical conductivity contribution of impurity phases such as CuO and/or oxygen vacancy.

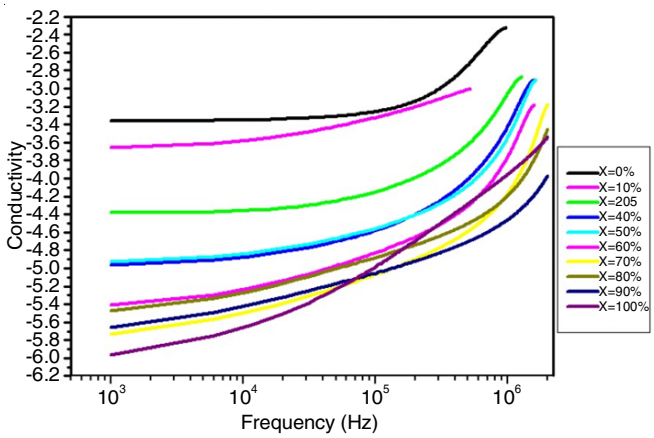

Fig. 7. Variation of conductivity as function of frequency for (1-x) CCTO-x PT (x = 0-100%) ceramics at 320 °C

The conductivity of these composites *versus* frequency follow the Jonscher's law.

The Cole-Cole (Z″ *versus* Z′) plot of these composites is fitted using a combination of R-C (in parallel) in series with R-CPE (in parallel) is shown in Fig. 8 (inset). The complex impedance Z* is related to the grain and grain-boundary parameters by the equation $Z^* = (R_g^{-1} + j\omega C_g)^{-1} + (R_{gb}^{-1} + j\omega C_{gb})^{-1}$ [30], where R_b, C_b, R_{gb}, C_{gb} are the grain and grain boundary parameters. The Cole-Cole diagram (Fig. 8) shows the presence of two semi-circles. The first one attributed to the grain effect while the second is related to the grain boundary effect.

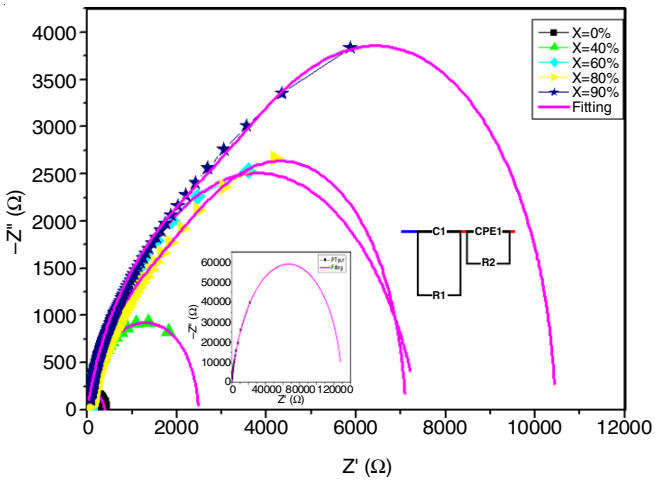

Fig. 8. Variation of Z′ as function of Z″ for (1-x) CCTO-x PT (x = 0-100%) ceramics at 320 °C

The grain boundaries resistance can be determined by the intersection of semi-circle with Z″ axis in high frequency region. It is found that the grain boundary resistance increases with the increase of PT content. The same behaviour is also observed for the grain resistance accompanied with the increase in conductivity. The center of semi-circles is on the real impedance axis, suggesting that the relaxation is of Debye type.

Conclusion

The structural and dielectric properties of CCTO-PT composite materials have been investigated. The Rietveld refinement

showed a predominant of tetragonal phase (PT phase) in benefit of cubic phase (CCTO phase) with the increase of PT content. Raman results also confirmed the XRD results, whereas the SEM images show a change in grain form from quadratic to semi-spherical and a grain size reduction with the increase in the PT content. The dielectric measurements have been investigated as function of temperature and showed two dielectric anomalies with a relaxation behaviour and present a diffuse character. And the electrical properties show that the conductivity decreases and the resistance of grain boundaries increases with the increase of lead titanate (PT) addition.

CONFLICT OF INTEREST

The authors declare that there is no conflict of interests regarding the publication of this article.

REFERENCES

1. J. Liu, R.W. Smith and W.-N. Mei, *Chem. Mater.*, **19**, 6020 (2007); https://doi.org/10.1021/cm0716553
2. T. Badapanda, R. Harichandan, S. Nayak, A. Mishra and S. Anwar, *Process. Appl. Ceram.*, **8**, 145 (2014); https://doi.org/10.2298/PAC1403145B
3. W. Li and R.W. Schwartz, *Appl. Phys. Lett.*, **90**, 112901 (2007); https://doi.org/10.1063/1.2713167
4. V.S. Vinila, R. Jacob, A. Mony, H.G. Nair, S. Issac, S. Rajan, A.S. Nair, D.J. Satheesh and J. Isac, *J. Cryst. Struct. Theory Appl.*, **3**, 57 (2014); https://doi.org/10.4236/csta.2014.33007
5. N. Hadi. T. Lamcharfi. F. Abdi and A. Elbasset, *Int. J. Dev. Res.*, **4**, 12432 (2017).
6. P.R. Bueno, W.C. Ribeiro, M.A. Ramírez, J.A. Varela and E. Longo, *J. Appl. Phys. Lett.*, **90**, 142912 (2007); https://doi.org/10.1063/1.2720301
7. M. Subramanian, D. Li, N. Duan, B.A. Reisner and A.W. Sleight, *Solid State J. Chem.*, **151**, 323 (2000); https://doi.org/10.1006/jssc.2000.8703
8. C.C. Homes, T. Vogt, S. M. Shapiro, S. Wakimoto, M. A. Subramanian, and A.P. Ramirez, *Phys. Rev. B*, **67**, 092106 (2002); https://doi.org/10.1103/PhysRevB.67.092106
9. X. H. Zheng, J. Xiao, X. Huang, D.P. Tang and X.L. Liu, *J. Mater. Sci: Mater. Electron.*, **22**, 1116 (2011); https://doi.org/10.1007/s10854-010-0269-6
10. T. Yamamoto, H. Igarashi and K. Okazaki, *J. Am. Ceram. Soc.*, **66**, 363 (1982); https://doi.org/10.1111/j.1151-2916.1983.tb10050.x
11. A. Moulson and J.M. Herbert, Electroceramics. Materials, Properties, Applications. Chapman & Hall: London, pp 464 (1990).
12. A. Mansingh, *Mater. Thin Films*, **102**, 69 (2001); https://doi.org/10.1080/00150199008221466
13. A.M. Glass, *Science*, **235**, 1003 (1987); https://doi.org/10.1126/science.235.4792.1003
14. G. Burns and B.A. Scott, *Phys. Rev. B*, **7**, 3088 (1973); https://doi.org/10.1103/PhysRevB.7.3088
15. K. Limame, S. Sayouri, M.M. Yahyaoui, A. Housni and B. Jaber, *Phys. B. Conden. Matt.*, **494**, 26 (2016); https://doi.org/10.1016/j.physb.2016.04.026
16. J.S. Wright and L.F. Francis, *J. Mater. Res.*, **8**, 1712 (1993); https://doi.org/10.1557/JMR.1993.1712
17. G.R. Fox, J.H. Adair and R.E. Newnham, *J. Mater. Sci.*, **25**, 3634 (1990); https://doi.org/10.1007/BF00575398
18. Y. Ohara, K. Koumoto, T. Shimizu and H. Yanagida, *J. Mater. Sci.*, **30**, 263 (1995); https://doi.org/10.1007/BF00352160
19. J. Xue, D. Wan and J. Wang, *J. Mater. Letts.*, **39**, 364 (1999); https://doi.org/10.1016/S0167-577X(99)00036-1
20. B. Barbier, Ph.D. Thesis, Elaboration et caractérisation de condensateurs à base de $CaCu_3Ti_4O_{12}$ à forte permittivité relative pour l'électronique de puissance, T. Université Toulouse III-Paul Sabatier (2009).
21. K. Limame, Ph.D. Thesis, Elaboration par voie sol-gel e, caractérisation et modélisation des propriétés physiques des matériaux $PbTiO_3$ dopés au La», T. Université Sidi Mohammed Ben Abdellah (2007).
22. N. Kolev, R.P. Bontchev, M.A.J. Jacobson, V.N. Popov, V.G. Hadjiev, A.P. Litvinchuk and M.N. Iliev, *J. Phys. Rev. B*, **66**, 132102 (2002); https://doi.org/10.1103/PhysRevB.66.132102
23. C. Mingxiang, Ph.D. Thesis, Extrinsic Dielectric Relaxation of Colossal Dielectric Constant Material $CaCu_3Ti_4O_{12}$, Department of Applied Physics, Polytechnic University, Hong Kong (2011).
24. K. Chen, Y. Wu, J. Liao, J. Liao and J. Zhu, *J. Integr. Ferroelectr.*, **47**, 143 (2008); https://doi.org/10.1080/10584580802089023
25. J. Liu, R.W. Smith and W.-N. Mei, *J. Am. Chem. Soc.*, **19**, 6020 (2007); https://doi.org/10.1021/cm0716553
26. M. D. Fontana, H. Idrissi, G. E. Kugel and K. J. Wojcik, *J. Phys. Condens. Matter.*, **3**, 8695 (1991); https://doi.org/10.1088/0953-8984/3/44/014
27. F. Li, S.J. Zhang, T.N. Yang, Z. Xu, N. Zhang, G. Liu, J. Wang, J. Wang, Z. Cheng, Z.-G. Ye, J. Luo, T.R. Shrout and L.-Q. Chen, *J. Nat Commun*, **7**, 13807 (2016); https://doi.org/10.1038/ncomms13807
28. Y. Dong, Z. Zhou, R. Liang and X. Dong, *J. Am. Ceram. Soc.*, **103**, 4785 (2020); https://doi.org/10.1111/jace.17174
29. V. Buscaglia, M.T. Buscaglia, M. Viviani, L. Mitoseriu, P. Nanni, V. Trefiletti, P. Piaggio, I. Gregora, T. Ostapchuk, J. Pokorny and J. Petzelt, *J. Eur. Ceram. Soc.*, **26**, 2889 (2006); https://doi.org/10.1016/j.jeurceramsoc.2006.02.005
30. Z. Yao, H. Liu, H. Hao and M. Cao, *J. Appl. Phys.*, **109**, 014105 (2011); https://doi.org/10.1063/1.3525995